Springer

KSME

Journal of Mechanical Science and Technology 28 (1) (2014) 255~261
www.springerlink.com/content/1738-494x
DOI 10.1007/s12206-013-0981-2

A kinetic decomposition process for air-gap interconnects and induced deformation instability of a low-k dielectric cap layer[†]

Suk-Kyu Ryu[1,3,*], Jay Im[2], Paul S. Ho[2] and Rui Huang[1]

[1]*Department of Aerospace Engineering and Engineering Mechanics, University of Texas, Austin, TX 78712, United States*
[2]*Microelectronics Research Center, University of Texas, Austin, TX 78712, United States*
[3]*Applied Materials, Inc., Santa Clara, CA 95054, United States*

(Manuscript Received February 9, 2013; Revised July 11, 2013; Accepted August 21, 2013)

Abstract

During air-gap formation in interconnects, decomposition process of the sacrificial layer induces deformation of a low-k dielectric cap layer. For analysis of ensuing structural instability, a logistic kinetics model is introduced to describe the removal process of the sacrificial layer, and finite difference method (FDM) is applied to evaluate the deformation behavior of the cap layer. The instability of the cap layer depends on its span length and the degree of adhesion between the cap layer and sacrificial layer. During decomposition, strong adhesion causes the collapse of the cap layer, while the cap deformation remains small and stable with weak adhesion. For intermediate adhesion, a snap-back instability is predicted as the cap layer suddenly detaches from the sacrificial layer at a critical deflection. The critical adhesion energy is predicted as a function of the air gap width.

Keywords: Air-gap; Interconnects; Instability; Adhesion; Failure; Thermal stress; Finite difference method (FDM)

---

1. Introduction

Continuous scaling of microelectronic devices has brought serious challenges to the material and process development of on-chip interconnects beyond the 32 nm technology node [1, 2]. In particular, interconnect RC delay becomes a main factor limiting the chip density and performance. To improve the RC delay in interconnects, low dielectric constant (low-k) materials were integrated in place of SiO_2. These low-k interconnects currently prevail in the microelectronics industry [3-6]. However, recently the trend of introducing various low-k materials has faced difficulty to overcome the requirement of new generation of interconnects. Thus, implementation of air-gaps in the trench level has been demonstrated as an effective potential solution to replace ultra low-k dielectrics [7, 8]. The air-gap structures may be produced by non-conformal chemical vapor deposition into patterned trenches, or by removing a sacrificial material [9-12]. However, air-gap interconnect confronts serious challenges concerning its structural integrity and mechanical stability due to process-induced thermal stresses as shown in Fig. 1 [13-18]. Figs. 1(b) and (c) are the collapse of the low-k cap (or hard mask) bridge over a wide gap during thermal decomposition of the gap forming material [7, 8, 12].

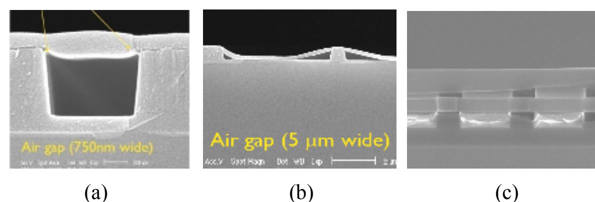

(a) (b) (c)

Fig. 1. Stability and reliability issues for air-gap structures [7, 12]: (a) delamination at the edge of air-gap; (b) and (c) collapse of low-k cap layer.

In this paper, the process of air-gap formation by removing a sacrificial material was studied. Decomposition of the sacrificial material was evaluated using a logistic kinetics model in order to establish the time dependent gap height. Here, we assumed that the decomposed gases escaped through a low-k interlayer dielectric (ILD), which acted as a cap layer. Deformations of the cap and the sacrificial layer during decomposition were investigated by taking into account the interaction forces. Finally, by employing finite difference method (FDM) [19], the effect of the interactive adhesion levels (strong, intermediate, and weak) on the detachment behavior of the cap layer from the residual sacrificial material was evaluated with respect to span length of the cap layer.

*Corresponding author. Tel.: +1 512 674 5763
E-mail address: sukkyuryu@gmail.com
† Recommended by Associate Editor Jong Soo Ko
© KSME & Springer 2014

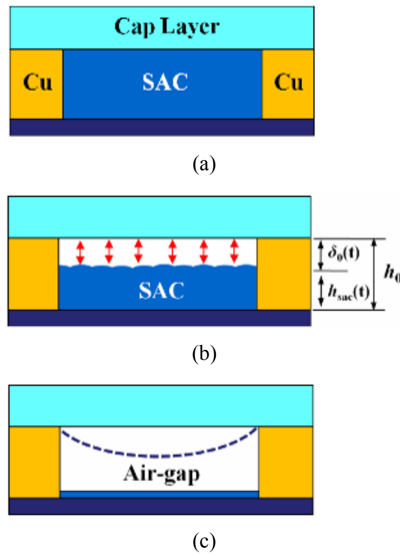

Fig. 2. Illustration of decomposition process for sacrificial material: (a) initial deposit status; (b) degradation of sacrificial layer; (c) air-gap formation (dash line indicates the deformation of cap layer).

2. Decomposition process of sacrificial layer

For air-gap formation, thermally degradable polymers may be used as a sacrificial material in between the metal lines. In the processing, the degradable polymer is deposited first, followed by trench formation by lithographic process, and Cu deposition into the trench. After removing the Cu overburden by chemical mechanical polishing (CMP), porous interlayer dielectric (ILD) is deposited. Then the sacrificial polymer is thermally decomposed and the gaseous by-product generated diffuses out through the porous ILD layer to complete the air-gap process [7]. Several kinetic models have been developed to explain the complex chemical decomposition processes [20]. In this study, the following logistic kinetics model is applied for numerical simplicity and stability [21].

$$C(t) = C_f + \frac{C_0 - C_f}{1 + \left(t / t_{50}\right)^n} \tag{1}$$

where $C(t)$ is the percentage of the remaining sacrificial material at time t. C_0 is the initial percentage, C_f is the final percentage, and t_{50}, n are the convergence parameters.

In the decomposition process, the sacrificial material is assumed to be uniformly removed starting from its upper surface in contact with the porous ILD cap layer, through which the decomposed gases will escape. The decomposition and removal of the sacrificial material lead to a separation between the cap layer and the sacrificial material. During this separation as a function of time t, interaction forces between the upper cap layer and lower sacrificial layer are generated due to adhesive energy as illustrated in Fig. 2. The detailed relationship between energy and force will be treated in the later section.

The thickness of the remaining sacrificial material at time t is defined as h_{sac}.

$$h_{sac}(t) = C(t) h_0 \tag{2}$$

where h_0 is the initial thickness.

As the sacrificial material degrades over time, the interfacial average separation (δ_0) between the cap and the sacrificial layer can be expressed as,

$$\delta_0(t) = h_0 - h_{sac}(t) = \left[1 - C(t)\right] h_0 \ . \tag{3}$$

At close proximity, two surfaces interact and exert forces onto each other (J. Israelachvili, *Intermolecular and Surface Forces*, Academic Press, 1992). Various physical origins for forces between surfaces exist, such as dispersion forces (Van der Waals), electrostatic forces, and hydration forces, etc.. To begin with, we assume a Lennard-Jones (L-J) type interaction [22] between the cap layer and the sacrificial layer. The interaction is described by L-J potential as a function of the surface separation,

$$U(\delta) = -\frac{4}{3}\Gamma\left[\left(\frac{r_0}{r_0+\delta}\right)^2 - \frac{1}{4}\left(\frac{r_0}{r_0+\delta}\right)^8\right]. \tag{4}$$

The interaction force (per unit area of the surface) is then

$$p(\delta) = -\frac{dU}{d\delta} = \frac{8\Gamma}{3r_0}\left[\left(\frac{r_0}{r_0+\delta}\right)^3 - \left(\frac{r_0}{r_0+\delta}\right)^9\right]. \tag{5}$$

Here, Γ is the adhesion energy between the two surfaces [23], and r_0 is a characteristic length that controls the decay of the interaction force as the surfaces are increasingly separated.

Typical values are 0.1-1 J/m^2 for Γ and about 1-5 nm for r_0. The force intensity varies from repulsive ($p < 0$) at negative separation ($\delta < 0$) to zero at zero separation and to attractive ($p > 0$) at positive separation ($\delta > 0$). The attractive interaction force reaches a maximum, $p_m = 16\Gamma / 9\sqrt{3} r_0$ at $\delta = 0.2r_0$, and then decays to become vanishingly small for $\delta > 10r_0$. Thus, the length r_0 sets the range of the interaction.

3. Mechanical model for cap layer deformation

3.1 Deformation of the cap layer: a beam model

As the sacrificial material is removed, separation of the two surfaces induces an attractive interaction force acting on the lower surface of the cap layer. Assume the upper surface of the cap layer is traction-free during the decomposition process. For a relatively wide air gap ($L/h_{cap} > 5$, where L and h_{cap} are the width and thickness of cap layer, respectively), we model the cap layer as a beam, for which the equilibrium equation is

$$\frac{E_{cap}h_{cap}^3}{12}\frac{\partial^4 w}{\partial x^4} - \sigma_0 h_{cap}\frac{\partial^2 w}{\partial x^2} = p \quad (6)$$

where w is the lateral deflection of the cap layer (positive towards the sacrificial layer), and x is the coordinate along the interface or gap. E_{cap} is the elastic modulus, h_{cap} is the cap layer thickness, and σ_0 is the residual stress in the cap layer (e.g., process-induced thermal stress).

Assuming that the cap layer is fixed at both ends (bonded to the neighboring Cu barriers), the deflection w at each time instance t is a function of x, which must satisfy the boundary conditions at the ends:

$$w = 0 \text{ and } \partial w/\partial x = 0 \text{ at } x = 0 \text{ and } L \quad (7)$$

with L being the length of the cap layer (or width of the air gap).

3.2 Deformation of the sacrificial layer: a Winkler model

The same interaction force also acts on the sacrificial layer and leads to elastic deformation. Assume that the lower surface of the sacrificial layer remains bonded to the substrate. The displacement of the upper surface is related to the interaction force by the Winkler model (simple elastic foundation) [24, 25]:

$$v = \frac{p h_{sac}}{E_{sac}} = \frac{h_0}{E_{sac}} C(t) p \quad (8)$$

where, v is the normal displacement (positive toward the cap layer), and E_{sac} is the elastic modulus of the sacrificial material.

3.3 Coupling of decomposition and deformation

At each time instance t, the surface separation between the cap layer and the remaining sacrificial layer depends on both the material removal and the deformation, the latter being a function of x. The total separation is thus

$$\delta(x, t) = \delta_0(t) - w(x, t) - v(x, t). \quad (9)$$

Here, δ_0(t) is as expressed in Eq. (3), and the displacements are related to the interaction force by Eqs. (6) and (8). Moreover, the local separation $\delta(x, t)$ is related to the interaction force by Eq. (5). The model system is thus complete, coupling the kinetic decomposition process with the surface interaction and elastic deformation of the cap layer and the sacrificial layer.

4. Finite difference methods (FDM)

The kinetic process as given by Eq. (1) and the interfacial interaction by Eq. (5) are nonlinear. Numerical solutions to the nonlinear system are sought by the following methods. For the purpose, we introduced a finite difference method (FDM) to simulate the coupled decomposition-deformation process. Using the finite difference method, the equation can be approximated by a matrix operation in the discrete form,

$$\boldsymbol{p} = \mathbf{D}\boldsymbol{w}. \quad (10)$$

Here, $\boldsymbol{p}$ and $\boldsymbol{w}$ are the vectors for the interaction force and deflection at discrete nodes, and $\mathbf{D}$ is a square matrix in Eq. (11), where Δx is the distance between two neighboring nodes, namely, the element size.

$$\mathrm{D} = \frac{\mathrm{E}_{cap} h_{cap}^3}{12(\Delta x)^4}\begin{bmatrix} 7 & -4 & 1 & 0 & 0 & 0 & 0 & 0 \\ -4 & 6 & -4 & 1 & 0 & 0 & 0 & 0 \\ 1 & -4 & 6 & -4 & 1 & 0 & 0 & 0 \\ 0 & 1 & -4 & 6 & -4 & 1 & 0 & 0 \\ 0 & \ddots & \ddots & \ddots & \ddots & \ddots & \ddots & 0 \\ 0 & 0 & 0 & 1 & -4 & 6 & -4 & 1 \\ 0 & 0 & 0 & 0 & 1 & -4 & 6 & -4 \\ 0 & 0 & 0 & 0 & 0 & 1 & -4 & 7 \end{bmatrix} - \frac{\sigma_0 h_{cap}}{(\Delta x)^2}\begin{bmatrix} -2 & 1 & 0 & 0 & 0 & 0 & 0 & 0 \\ 1 & -2 & 1 & 0 & 0 & 0 & 0 & 0 \\ 0 & 1 & -2 & 1 & 0 & 0 & 0 & 0 \\ 0 & 0 & 1 & -2 & 1 & 0 & 0 & 0 \\ 0 & \ddots & \ddots & \ddots & \ddots & \ddots & \ddots & 0 \\ 0 & 0 & 0 & 0 & 1 & -2 & 1 & 0 \\ 0 & 0 & 0 & 0 & 0 & 1 & -2 & 1 \\ 0 & 0 & 0 & 0 & 0 & 0 & 1 & -2 \end{bmatrix}. \quad (11)$$

The second term in the square matrix comes from residual stress (σ_0). However, for simplicity, we first ignored the process-induced residual stress in the cap layer, i.e., $\sigma_0 = 0$. Then Eq. (6) becomes a linear differential equation. The effect of residual stress currently ignored will be discussed later in next section. Note that the boundary conditions for the deflection have been applied for the end nodes. Similarly, Eq. (8) can be written in a matrix form:

$$v = \frac{h_0 - \delta_0(t)}{E_{sac}} \mathrm{I}\, p = \frac{h_0}{E_{sac}} C(t) \mathrm{I}\, p \quad (12)$$

where, $\mathbf{I}$ is the identity matrix of the same size as $\mathbf{D}$.

In Eq. (12), $C(t)$ is a nonlinear function of time t. An incremental form of Eq. (12) is

$$\begin{aligned} \Delta v &= \frac{h_0 - \delta_0(t+\Delta t)}{E_{sac}}\left(p + \Delta \mathrm{p}\right) - \frac{h_0 - \delta_0(t)}{E_{sac}}\mathrm{p} \\ &= \frac{1}{E_{sac}}\left[\left(\delta_0(t) - \delta_0(t+\Delta t)\right)\mathrm{p} + (h_0 - \delta_0(t+\Delta t))\Delta \mathrm{p}\right]. \end{aligned} \quad (13)$$

Eq. (5) gives a nonlinear relationship between p and δ at each node. The increments, Δp and $\Delta\delta$, from time t to $t+\Delta t$ are related approximately by a linear relation,

$$\Delta \mathrm{p} = \mathrm{K}\,\Delta\delta \tag{14}$$

where **K** is a diagonal matrix: $\mathrm{K}_{mm} = \mathrm{K}(\delta_m) = (dp/d\delta)_{\delta_m}$, and δ_m is the surface separation at node m.

$$\mathrm{K}(\delta) = \frac{dp}{d\delta} = -\frac{8\Gamma}{r_0^2}\left[\left(\frac{r_0}{r_0+\delta}\right)^4 - 3\left(\frac{r_0}{r_0+\delta}\right)^{10}\right]. \tag{15}$$

Incremental deflection, Δw, can be obtained from Eq. (10) as,

$$\Delta w = \mathbf{D}^{-1}\Delta \mathrm{p}. \tag{16}$$

In addition, Eq. (9) can be rewritten in a matrix and incremental form,

$$\Delta\delta = \Delta\delta_0 - \Delta w - \Delta v. \tag{17}$$

Substituting Eqs. (13), (14), and (16) into Eq. (17), we obtain that

$$\left[\mathrm{K}^{-1} + \mathrm{D}^{-1} + \frac{1}{E_{sac}}(h_0 - \delta_0(t+\Delta t))\,\mathrm{I}\right]\Delta \mathrm{p} = \Delta\delta_0 - \frac{1}{E_{sac}}\left(\delta_0(t) - \delta_0(t+\Delta t)\right)\mathrm{p}. \tag{18}$$

It was found that the matrix **K** sometimes becomes ill-conditioned and the calculation of its inverse causes a divergence problem. This may be mitigated by an alternative form of Eq. (18):

$$\left[\mathrm{I} + \mathrm{D}^{-1}\mathrm{K} + \frac{1}{E_{sac}}(h_0 - \delta_0(t+\Delta t))\,\mathrm{K}\right]\Delta\delta = \Delta\delta_0 - \frac{1}{E_{sac}}\left(\delta_0(t) - \delta_0(t+\Delta t)\right)\mathrm{p}. \tag{19}$$

A normalized form of Eq. (19) is then

$$\left[\mathrm{I} + \overline{\mathrm{D}}^{-1}\overline{\mathrm{K}} + (1 - \overline{\delta_0}(t+\Delta t))\,\overline{\mathrm{K}}\right]\Delta\overline{\delta} = \Delta\overline{\delta}_0 - \left(\overline{\delta_0}(t) - \overline{\delta_0}(t+\Delta t)\right)\overline{\mathrm{p}} \tag{20}$$

where the separations are normalized by thickness h_0, the pressure is normalized by the modulus E_{sac}, and both **K** and **D** are normalized by E_{sac}/h_0.

The kinetics model gives $\Delta\delta_0$ for every time increment. Then, solve Eq. (20) to find $\Delta\delta$, and the other increments, Δp, Δw, and Δv, from Eqs. (14), (16) and (13), respectively. After updating the quantities, repeat the above steps for the next time increment.

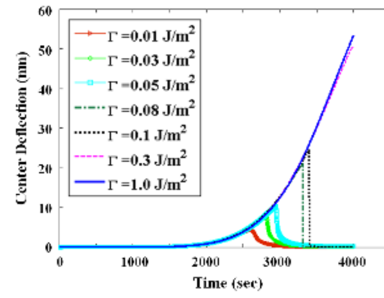

Fig. 3. Center deflection of the cap layer as a function of time for different adhesion energies.

Steps:

(0) construct matrix **D** (out of the loop).

(1) calculate **K** (in the loop).

(2) calculate normalized separation increment.

$$\Delta\overline{\delta} = \left[\mathrm{I} + \overline{\mathrm{D}}^{-1}\overline{\mathrm{K}} + (1 - \overline{\delta_0}(t+\Delta t))\overline{\mathrm{K}}\right]^{-1}\left[\Delta\overline{\delta}_0 - \left(\overline{\delta_0}(t) - \overline{\delta_0}(t+\Delta t)\right)\overline{\mathrm{p}}\right].$$

(3) calculate other parameters

$\Delta\overline{\mathrm{p}} = \overline{\mathrm{K}}\,\Delta\overline{\delta}$,

$\Delta\overline{w} = \overline{\mathrm{D}}^{-1}\,\Delta\overline{\mathrm{p}}$,

$\Delta\overline{\mathrm{v}} = \left(\overline{\delta_0}(t) - \overline{\delta_0}(t+\Delta t)\right)\overline{\mathrm{p}} + (1 - \overline{\delta_0}(t+\Delta t))\Delta\overline{\mathrm{p}}$.

(4) update δ, p, w, v.

(5) repeat (1)-(4).

5. Effect of adhesion strength on structural instability

It is found that the separation and deformation during the decomposition process strongly depend on the adhesion energy Γ between the cap layer and the sacrificial layer. Three distinct modes of behavior are identified for large, intermediate, and small adhesion energies, respectively. As illustrated in Fig. 5 for various Γ, the deflections at the center of the cap layer are very different. In these calculations, we have set r_0 = 5 nm, h_0 = 110 nm, h_{cap} = 110 nm, E_{cap} = 9.5 GPa, E_{sac} = 6 GPa, L = 1 μm and the residual stress is neglected (σ_0 = 0) for a simple evaluation. In addition, we set n = 7 and t_{50} = 4000 sec for the logistic kinetics model. Fig. 3 indicates that the separation and deformation during the decomposition process strongly depend on the adhesion energy.

5.1 Adhesive energy

Fig. 4 shows the distribution and evolution of the cap layer deformation (h_{sac}-w), surface separation (δ), and the interaction force (p) at different time instances of the decomposition process, for the case of strong adhesion (Γ = 1 J/m^2). For strong adhesion, the center of the cap layer is stuck to the sacrificial layer all the time as shown in Fig. 4(b). The center deflection increases as the decomposition continues and reaches over 100 nm at the end of the decomposition process.

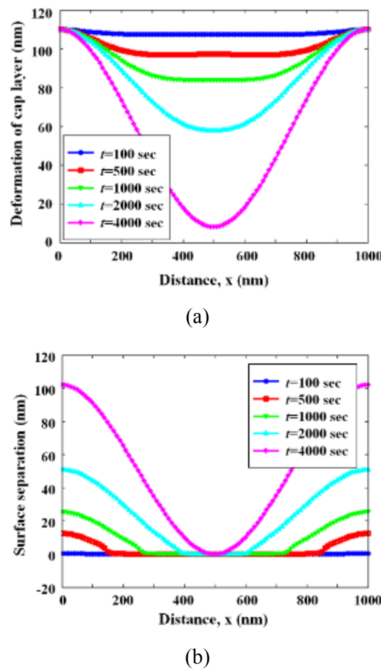

Fig. 4. Structural instability for strong adhesive energy (Γ = 1 J/m^2): (a) deformation of the cap layer; (b) surface separation between the cap and the sacrificial layer.

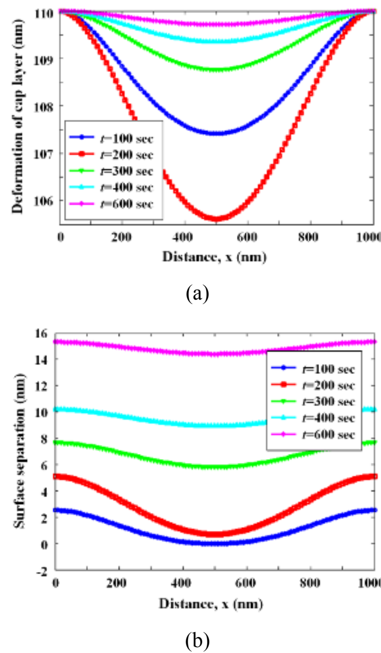

Fig. 5. Structural instability for weak adhesive energy (Γ = 0.01 J/m^2): (a) deformation of the cap layer; (b) surface separation between the cap and the sacrificial layer.

In this case, the deflection of the cap layer is significant and could cause collapse of the cap due to failure at the ends.

Fig. 5 shows the behaviors for weak adhesion (Γ = 0.01 J/m^2). For weak adhesion, the center of the cap layer deflects slightly (up to about 5 nm) at the beginning of the decomposition process and then smoothly retreats back as the surfaces are further separated with continual decomposition. In this case, the interaction between the cap layer and the sacrificial layer is weak and collapse of the cap is unlikely.

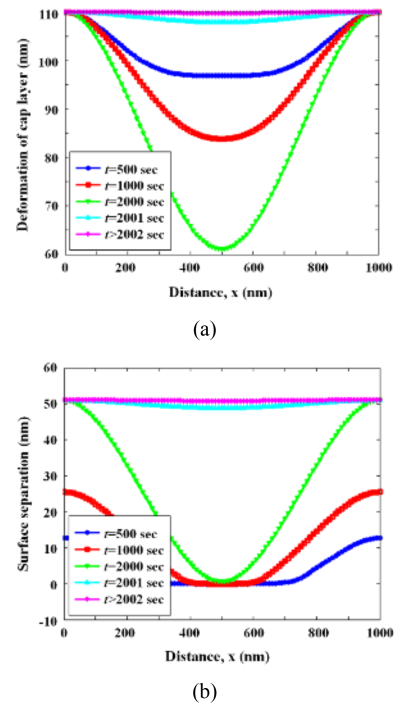

Fig. 6. Structural instability for intermediate adhesive energy (Γ = 0.1 J/m^2): (a) deformation of the cap layer; (b) surface separation between the cap and the sacrificial layer.

For intermediate adhesion (Γ = 0.1 J/m^2), the center of the cap layer deflects until it reaches a point of instability and then snaps back abruptly to zero deflection (Fig. 6). The point of instability depends on the adhesion energy as well as the modulus and thickness of the cap layer. The snap transition may lead to a dynamic deformation process (e.g., vibration). Depending on the level of the maximum deflection, collapse of the cap layer may occur.

5.2 Effect of various lengths of the cap layer

Considering the intermediate adhesion (Γ = 0.1 J/m^2), the effect of different length of the cap layer on the deformation is also studied. For a relatively short length of the cap layer, the interaction force eventually becomes very weak after 4000 sec so that the cap layer retreats back almost to the original position. However, as the length of the cap layer is increasing, the interaction force seems to be stronger at the center of the cap layer (Fig. 7(a)). In Fig. 7(b), the interaction force doesn't become zero at the center of cap. Thus, the center deflection of cap layer also doesn't completely return to its initial position, either. From the above results, we might find the threshold adhesive energy of layer detachment with respect to the length of the cap layer.

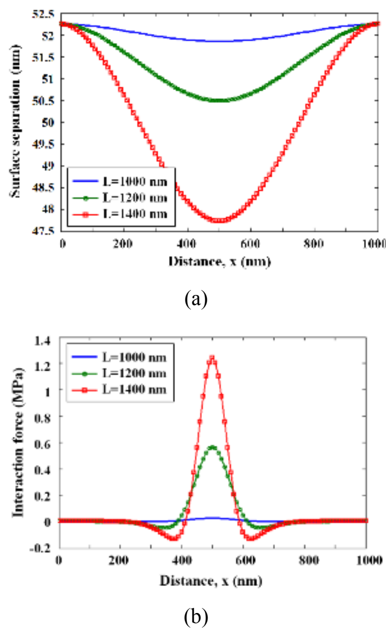

Fig. 7. (a) Surface separation; (b) interaction force for different lengths of cap layer for intermediate adhesion at t = 4000 sec.

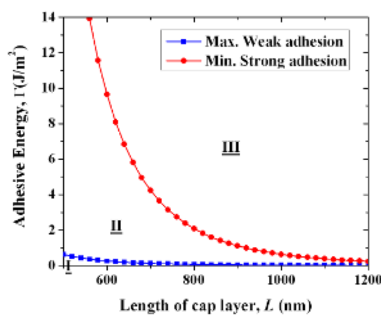

Fig. 8. Critical adhesion energies for various lengths of the cap layer.

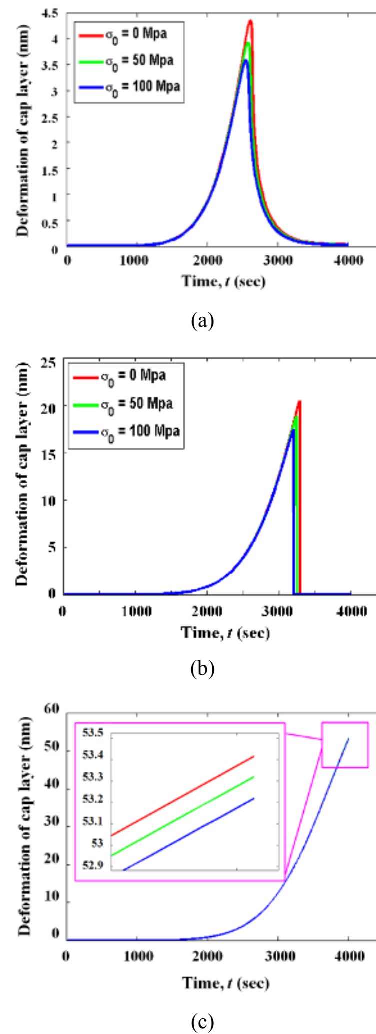

Fig. 9. The effect of process-induced residual stress: (a) Γ = 0.01 J/m^2; (b) Γ = 0.1 J/m^2; (c) Γ = 1 J/m^2.

Fig. 8 shows the critical adhesion energies for various lengths of the cap layer. In this plot, the first region (I) below the blue line with square symbol corresponds to weak adhesion and the second area above the red line with circle symbol (III) is for strong adhesion. The last region in between two lines (II) indicates the case of intermediate adhesion. For a relatively short length of cap layer, the behavior was mostly that of intermediate adhesion; that is, sudden detachment of the adhering layers. However, as the cap layer length increases, the mode of detachment behavior becomes very sensitive to the level of adhesive energy. The result can serve as a design guideline for the air-gap interconnects.

5.3 Effect of residual stress

As a last part, the effect of residual stress, σ_0 previously ignored in section 5.1 was investigated with the same numerical model. The trend of center deflection including σ_0 up to 100 MPa was similar to the previous cases where the residual stress term was neglected (Fig. 9). Even though the effect of the residual stress is small, the cap layer deflection still becomes smaller when the intensity of residual stress increases, due to the reversely increasing bending effect of residual stress.

6. Conclusions

A kinetics model is introduced to simulate the removal process of the sacrificial layer to form air-gap interconnects. The decomposition process of the sacrificial layer is analyzed by numerical methods. The induced deformation of a low-k cap layer depends on its span length between the Cu channels and the degree of adhesion between the cap layer and sacrificial layer.

For strong adhesion energy, the center of cap layer always bonds to the sacrificial layer in spite of a large deflection. This implies that the cap layer can ultimately be ‘collapsed’ under this condition. However, the behavior at weak adhesion appears stable. The cap layer smoothly deflects and retreats back.

For intermediate adhesion, the cap layer suddenly returns to the original position with a snap-back motion after some deflection. Under this condition, dynamic force is exerted, which might cause layer cracking near the fixed edge of the cap layer. The distinction among the different levels of adhesion is diminished if the cap layer span length is reduced; the behavior was akin to a case of intermediate adhesion.

References

[1] B. Li, T. D. Sullivan, T. C. Lee and D. Badami, Reliability challenges for copper interconnects, *Microelectronics Reliability*, 44 (3) (2004) 365-380.

[2] M. T. Bohr, Interconnect scaling-the real limiter to high performance ULSI, *International Electron Devices Meeting* (1995) 241-244.

[3] Y. J. Ma, H. N. Yang and J. Guo, Structural and electronic properties of low dielectric constant fluorinated amorphous carbon films, *Applied Physics Letters*, 72 (25) (1998) 3353-3355.

[4] H. Treichel et al., Low dielectric constant materials for interlayer dielectric, *Microelectronic Engineering*, 40 (1) (1998) 1-19.

[5] H. Zhou, F.G. Shi, B. Zhao and J. Yota, Effect of deposition methods on dielectric breakdown strength of PECVD low-k carbon doped silicon dioxide dielectric thin films, *Microelectronics Journal*, 35 (7) (2004) 571-576.

[6] G. Bomchil, A. Halimaoui and R. Herino, Porous silicon: The material and its applications in silicon-on-insulator technologies, *Applied Surface Science*, 41-42 (0) (1989) 604-613.

[7] R. Hoofman, R. Daamen, J. Micheton and V. Nguyenhoang, Dielectric air-gap integration, *Solid State Technology* (2006) 55-58.

[8] S. Nitta et al., A multi level copper/low-k/airgap BEOL technology, *Advanced Metallization Conference* (2008) 329-336.

[9] L. G. Gosset et al., Advanced Cu interconnects using air gaps, *Microelectronic Engineering*, 82 (3-4) (2005) 321-332.

[10] S. Uno et al., Sacrificial CVD film etch-back process for air-gap Cu interconnects, *Thin Solid Films*, 515 (12) (2007) 4960-4965.

[11] W. Kronast et al., Single-chip condenser microphone using porous silicon as sacrificial layer for the air gap, *Sensors and Actuators A: Physical*, 87 (3) (2001) 188-193.

[12] S. Park, S. A. B. Allen and P. A. Kohl, Air-gaps for high-performance on-chip interconnect part I: Improvement in thermally decomposable template. *Journal of Electronic Materials*, 37 (10) (2008) 1524-1533.

[13] F. Gaillard et al., Chemical etching solutions for air gap formation using a sacrificial oxide/polymer approach, *Microelectronic Engineering*, 83 (11-12) (2006) 2309-2313.

[14] J. Noguchi et al., Process and reliability of air-gap Cu interconnect using 90-nm node technology, *IEEE Transactions on Electron Devices*, 52 (3) (2005) 352-359.

[15] X. F. Zhang et al., Mechanical stability study of air-gap interconnects, *Future Fab International*, 27 (2008) 81-87.

[16] S. K. Ryu et al, Impact of near-surface thermal stresses on interfacial reliability of through-silicon-vias for 3-D interconnects, *IEEE Trans. on Device and Materials Reliability*, 11 (1) (2011) 35-43.

[17] S. K. Ryu et al., Characterization of thermal stresses in through-silicon vias for three-dimensional interconnects by bending beam technique, *Applied Physics Letters*, 100 (2012) 041901-1-04190-4.

[18] S. K. Ryu et al., Micro-raman spectroscopy and analysis of near-surface stresses in silicon around through-silicon vias for three-dimensional interconnects, *J. Appl. Phys.*, 111 (6) (2012) 063513 - 063513-8.

[19] D. S. Sankar and Usik Lee, FDM analysis for MHD flow of a non-Newtonian fluid for blood flow in stenosed arteries, *J. of Mechanical Science and Technology*, 25 (10) (2011) 2573-2581.

[20] Y. Kodera, Distribution kinetics of polymer thermogravimetric analysis: A model for chain-end and random scission, *Energy & Fuels*, 16 (2002) 119-126.

[21] X. Zhang et al., Impact of process induced stressed and chip-packaging interactive on reliability of air-gap interconnects, *proceedings of the IEEE International Interconnect Technology Conference* (IITC 2008), June 2-4 (2008).

[22] R. M. Springman and J. Bassani, Snap transitions in adhesion, *J. Mech. Phys. Solids*, 56 (6) (2008) 2358-2380.

[23] J. O. Aguilar et al., Adhesion strength in laminated glazings containing multilayer solar control coatings, *J. of Mechanical Science and Technology*, 26 (6) (2012) 1725-1730.

[24] A. M. Zenkour and M. Sobhy, Elastic foundation analysis of uniformly loaded functionally graded viscoelastic sandwich plates, *Journal of Mechanics*, 28 (3) (2012) 439-452.

[25] J. Jumel, M. K. Budzik and M. E. R. Shanahan, Beam on elastic foundation with anticlastic curvature: Application to analysis of mode I fracture tests, *Engineering Fracture Mechanics*, 78 (18) (2011) 3253-3269.

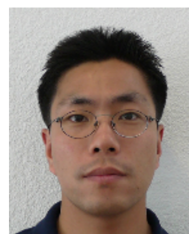

Suk-Kyu Ryu received the B.S. and M.S. degrees in aerospace engineering from Korea Aerospace University, Korea, in 1998 and 2000, respectively, and the Ph.D. degree in Aerospace Engineering and Engineering Mechanics from The University of Texas, Austin, in 2011. He had several years of working experience in the composite material industry, and he was a research scientist in a micro system laboratory of Korea Institute of Science and Technology. Currently, he is a senior engineer at Applied Materials, CA. His research interests are the thermo-mechanical, process-related reliability issues in electronics materials & microelectronic packaging.